Hedgehog signaling controls progenitor differentiation timing during heart development

Authors: Megan Rowton[1], Andrew D. Hoffmann[1], Jeffrey D. Steimle[1], Xinan Holly Yang[1], Alexander Guzzetta[1], Sonja Lazarevic[1], Chul Kim[1], Nikita Deng[1], Emery Lu[1], Jessica Jacobs-Li[1], Shuhan Yu[1], Erika Hanson[1], Carlos Perez-Cervantes[1], Sunny Sun-Kin Chan[2], Kohta Ikegami[1], Daniel J. Garry[2], Michael Kyba[2], Ivan P. Moskowitz[1*].

Affiliations:

1. Departments of Pediatrics, Pathology, and Human Genetics, The University of Chicago, Chicago, Illinois, United States of America

2. Lillehei Heart Institute, University of Minnesota, Minneapolis, MN 55455, USA; Department of Pediatrics, University of Minnesota, Minneapolis, MN 55455, USA

[*] indicates corresponding author: imoskowitz@peds.bsd.uchicago.edu

Abstract

A balance between progenitor cell maintenance and differentiation is tightly regulated during embryonic development[1-3] and adult tissue homeostasis[4-8]. Hedgehog (Hh) signaling is known to function within the progenitor cell populations of several developing[9] and regenerative[10] organs, and in cancers with resident progenitor subpopulations[11-12]. Here we provide evidence that Hh signaling dictates differentiation timing by promoting progenitor status and inhibiting differentiation during mammalian heart morphogenesis. Removal of active Hh signaling from cardiac progenitors *in vivo* caused increased cardiomyocyte differentiation gene expression, precocious differentiation, and Congenital Heart Disease (CHD). Modeling active Hh signaling through expression of the activating Hh transcription factor (TF), GLI1, in cardiac progenitors enabled the maintenance of a progenitor-specific regulatory network and delayed onset of the cardiomyocyte differentiation program. Progenitor-specific, but not differentiated cardiomyocyte-specific, accessible chromatin regions were enriched for GLI binding motifs. Furthermore, GLI1 expression promoted a global shift of chromatin accessibility towards progenitor-like, and away from cardiomyocyte-like, profiles at distal regulatory elements. The shift from active to repressive GLI TF abundance comprised a molecular switch that determined the activity patterns of progenitor-specific regulatory elements *in vitro* and *in vivo*. Thus, Hh signaling modulates a GLI switch at progenitor enhancers to activate progenitor gene expression and inhibit premature differentiation, thereby determining cardiac progenitor differentiation timing. This provides a novel molecular paradigm for progenitor maintenance by signal-dependent TFs with implications for organ development, regenerative potential, and cancer.

Main text

The vertebrate heart forms from two spatially distinct pools of cardiac progenitors that differentiate at different stages - the first heart field, which differentiates early into the embryonic heart tube (HT) and the second heart field (SHF), which differentiates later after migrating into the HT to form cardiac structures critical for mammalian cardiopulmonary circulation, including the right ventricle, pulmonary artery, and atrial septum (reviewed in [13]). The juxtaposition of SHF cardiac progenitors (blue region) and differentiating cardiomyocytes in the HT (red region) thus provides a unique system for investigating the spatiotemporal regulation of cardiomyocyte differentiation (Fig. 1a). Active Hh signal is sent from pulmonary endoderm to the adjacent SHF and is required in the SHF for the genesis of SHF-derived structures[14-16]. Hh signaling is excluded from the heart itself[14-15]. Hh signaling is effected by the nuclear accumulation of activating GLI TFs (GLI^A TFs: GLI1, $GLI2^A$, $GLI3^A$) at the expense of repressive GLI TFs (GLI^R TFs: $GLI2^R$, $GLI3^R$), however, the molecular mechanism by which GLI TFs direct cardiogenesis in cardiac progenitors of the SHF remains unclear.

We defined Hh-dependent SHF gene expression by performing transcriptional profiling of the pSHF from E10.5 *Shh* mutant ($Shh^{-/-}$) and littermate control ($Shh^{+/+}$) embryos. RNA-seq and confirmation with qPCR or *in situ* hybridization revealed downregulation of many genes expressed in embryonic mesoderm or cardiac progenitors, such as *Foxf1*, *Wnt2b*, *Snai1,* and *Osr1* and *Gli1*, a marker for Hh signaling itself (Fig. 1b, Extended Data Fig. 1a-d, f, g). Gene Ontology (GO) analysis of these genes identified terms including “smoothened signaling” and progenitor-specific developmental terms including “pattern formation”, “morphogenesis”, and

"regionalization" (Fig. 1d). In contrast, upregulated genes in the *Shh* mutant pSHF included cardiomyocyte differentiation products such as *Myl3*, *Tnni3* and *Nppa* (Fig. 1b, Extended Data Fig. 1a-b, e). GO analysis on upregulated genes identified terms associated with cardiomyocyte differentiation, including "muscle cell differentiation", "myofibril assembly", "sarcomere", "myofibrils", and "cardiac muscle tissue development" (Fig. 1d). These findings suggested that Hh signaling in the pSHF activated progenitor-specific gene expression but repressed cardiomyocyte differentiation-specific gene expression. Indeed, genes downregulated in the *Shh* mutant pSHF were normally more highly expressed in the pSHF compared with the HT, whereas genes upregulated were normally more highly expressed in HT compared with pSHF (Fig. 1c). These observations suggested that Hh signaling maintained progenitor gene expression and prevented cardiomyocyte differentiation gene expression in the pSHF.

We hypothesized that removal of Hh signaling from the SHF would affect cardiac progenitor differentiation status *in-vivo*. We observed precocious differentiation of the pSHF, based on the inappropriate expression of sarcomeric myosin (MF20) in the pSHF and lack of mesenchymal cells migrating into the heart from the pSHF (yellow arrowhead) in $Shh^{-/-}$ mice, compared to wild type littermate controls at E10.5 (Fig. 1e). $Shh^{-/-}$ embryos demonstrated CHD (atrioventricular septal defects) at E14.5, consistent with previous reports[17-20]. We predicted that Hh-dependent differentiation control in the SHF was exerted through Hh effector GLI TF activity. We predicted that ectopic GLI^R expression in the embryonic SHF would override GLI^A activity to cause precocious differentiation in the SHF and CHD. We induced constitutive expression of $GLI3^R$ from

the *ROSA26*$^{Gli3T\text{-}Flag\ c/c}$ allele[21] in the pSHF with tamoxifen-inducible Cre-recombinase expressed from the *Osr1*$^{eGFPCre\text{-}ERt2}$ allele[22], administering tamoxifen during SHF maturation from E7.5 – E9.5[15]. Indelible expression of *GLI3*^{R} in the pSHF (*Osr1*$^{eGFPCre\text{-}ERt2}$; *ROSA26*$^{Gli3T\text{-}Flag\ c/+}$*)* caused precocious differentiation of cardiomyocytes in the SHF, evidenced by increased expression of pSHF sarcomeric myosin (MF20) and lack of mesenchymal cells migrating into the IFT, relative to littermate controls at E10.5 (*ROSA26*$^{Gli3T\text{-}Flag\ c/+}$*;* Fig. 1e). Mutant embryos, but not littermate controls, demonstrated AVSDs at E14.5 (Fig. 4f). Together, these findings linked a disruption of GLI^{A} / GLI^{R} TF balance to structural heart defects and suggested that Hh signaling maintained SHF progenitor status by maintaining GLI^{A} TF predominance.

We utilized a mouse embryonic stem cell (mESC) system to investigate GLI TF control of cardiac differentiation timing[23] (Extended Data Fig. 2a). We evaluated baseline Hh signaling in a time course of mESC differentiation into cardiomyocytes. Active Hh signaling was observed in stem cells (Day -2-0) and early mesoderm (D2) based on the expression of Hh targets *Gli1* and *Ptch1*[24-26] and the relative protein ratios of GLI^{A} (GLI1, GLI3^{A}) to GLI^{R} (GLI3^{R}), which demonstrated a predominance of GLI^{A} by western blot (Extended Data Fig. 2b, d-g). In contrast, specified cardiomyocyte progenitors (Day 5-7) and differentiated cardiomyocytes (Day 8-12) demonstrated inactive Hh signaling, based on the reduction of *Gli1* and *Ptch1* expression and a predominance of GLI^{R} by western blot (Extended Data Fig. 2b, d-g). Quantification of the relative protein abundances of GLI^{A} (GLI1, GLI3^{A}) and GLI^{R} (GLI3^{R}) demonstrated a transition from active Hh signaling with high GLI^{A} to inactive Hh signaling with high GLI^{R} coincident with the onset of cardiomyocyte differentiation (Extended Data Fig. 2g).

We hypothesized that the transition from GLI^A to GLI^R TF predominance was required to promote cardiomyocyte differentiation and predicted that enforced GLI^A expression may prevent cardiomyocyte differentiation. We developed a doxycycline-inducible GLI1 overexpression (GLI1 OE) mESC line to enable GLI^A expression during cardiac differentiation *in vitro* (Extended Data Fig. 3a). To mimic the transient exposure of SHF cardiac progenitors to active Hh signaling experienced *in vivo*, we induced GLI1 expression for 24 hours in cardiac progenitor (CP) stage cells (Day 5-6; Fig. 2a). Doxycycline treatment resulted in activation of *Gli1* transcript and GLI1 protein, and the SHF Hh target gene *Foxf1*[16] within 24 hours (Extended Data Fig. 3b-d). Strikingly, transient GLI1 overexpression in cardiac progenitors (GLI1 OE) inhibited cardiomyocyte differentiation, reflected in a dramatic reduction in the expression of cardiac troponin (cTnT) and in the number of beating cardiomyocyte foci Day 8, compared to control cells (Fig. 2b-d). By Day 12 of differentiation, however, beating foci number and cTnT expression had recovered in GLI1 OE cells, compared to control cells (Fig. 2e-g). These observations indicated that transient activation of Hh signaling in cardiac progenitors resulted in delayed cardiac differentiation, not abrogated differentiation potential.

We investigated the effect of transient GLI1 OE in cardiac progenitors on the progenitor and differentiation gene expression programs in a temporal series of differentiation stages: cardiac progenitors (Day 6), early cardiomyocytes (Day 8) and late cardiomyocytes (Day 12). GLI1 OE caused a sharp and global increase in the expression of progenitor and mesoderm-specific genes, and a sharp decrease in the

expression of cardiomyocyte differentiation genes at Day 6 (Fig. 2h, j-k, Extended Data Fig. 4a-b). GO terms associated with genes induced by GLI1 at Day 6 included progenitor terms such as “developmental programs”, “cell division” and “growth factor activity”, while those associated with genes down-regulated by GLI1 OE included differentiation terms such as “differentiation”, “cardiomyopathy” and “the sarcomere” (Fig. 2h). After doxycycline was removed from the media and differentiation proceeded, both progenitor- and differentiation-specific gene expression levels normalized over time. The number of differentially expressed genes (logFC ≥ 1.5; FDR ≤ 0.05) decreased from 1,652 at Day 6 to 78 by Day 12, and the correlation between global transcriptional profiles of GLI1 OE and control cells increased (Fig. 2i, Extended Data Fig. 4a-b). By Day 12, expression levels of progenitor-specific genes *Gli1*, *Foxf1* and *Bra* in treated cells were similar to control cells, as were the expression levels of the cardiomyocyte differentiation genes *Tnnt2*, *Myh6* and *Hand2* (Fig. 2j-k). Collectively, these results suggest that transient GLI^A expression in cardiac progenitors temporarily prevented differentiation by up-regulating progenitor program genes and down-regulating cardiomyocyte differentiation program genes.

We hypothesized that GLI^A maintains cardiac progenitor status by promoting gene expression directly at progenitor-specific *cis*-regulatory elements (CREs). We identified candidate cardiac progenitor-specific and cardiomyocyte-specific *cis*-regulatory regions by comparing accessible chromatin regions in the embryonic pSHF and HT at E10 using ATAC-seq[27]. *De novo* motif analysis on pSHF-specific accessible regions revealed enrichment for binding sites of mesoderm and progenitor-specific transcription factors, such as TCF/LEF, HOXC10, and TWIST1, while HT-specific

regions were enriched for cardiac TF motifs, including GATA6, NKX2-5 and TBX5, indicating that chromatin organization in cardiac progenitors and cardiomyocytes reflects the distinct gene expression programs activated in each tissue (Fig. 3a). Importantly, we observed strong enrichment of GLI and GLI-similar (GLIS) binding motifs in pSHF-specific regions, relative to HT-specific regions (Fig. 3c, Hs GLI2 adjusted P-value = $3.74e^{-20}$). These results suggest that Hh signaling may direct a progenitor gene expression program in the pSHF through direct GLI^A regulation from CREs accessible in the progenitor state.

GLI^A motif enrichment at pSHF-specific accessible chromatin regions could reflect passive localization of GLI^A to previously accessible sites or GLI^A localization causing active chromatin remodeling and increased accessibility specifically in cardiac progenitors. We investigated the consequence of GLI^A expression on chromatin accessibility by comparing the ATAC-seq profile of GLI1 OE cardiac progenitors to control cells at Day 7. We found 8,001 newly accessible regions upon GLI1 OE in cardiac progenitors (Fig. 3b). *De novo* motif analysis of GLI1 OE-specific accessible chromatin regions revealed strong enrichment for Hh-dependent FOX TF motifs, while control-specific regions were enriched for motifs of blood and cardiac lineage-specifying TFs, including TAL1 and NKX2-5. Interestingly, GLI1 OE-specific regions were also enriched for ZFX and HIC1 binding motifs, two transcription factors known to cooperate with GLI TFs to prevent neuronal differentiation and propagate Hh-activated medulloblastoma[28-29]. Similar to pSHF-specific accessible regions, GLI1 OE-specific peaks were enriched for GLI binding motifs, relative to control cells (Fig. 3c). Strikingly, GLI1 OE-specific accessible chromatin regions were highly overrepresented in pSHF-

specific regions compared to HT-specific regions (Extended Data Fig. 5a), suggesting that GLI^A expression in cardiac progenitors *in vitro* promotes the global adoption of pSHF-like progenitor cell chromatin organization.

To investigate the progenitor-specific mechanism by which GLI^A controls the expression of Hh target genes, we examined the locations of accessible regions specific for GLI1 OE progenitors. Putative CREs near Hh-dependent genes containing known GLI binding sites[21] were transformed from inaccessible in control cells, as in the HT, to accessible, as in the pSHF, upon GLI1 OE (Fig. 3d green boxes, region upstream of the Hh target, *Ptch1*). While chromatin at the promoters of direct GLI1 targets, such as *Gli1* and *Foxf1*, were rendered more accessible upon GLI1 OE (Extended Data Fig. 5b-c), we observed that the majority of chromatin reorganization occurred at regions distal to transcriptional start sites (Fig. 3e). We therefore examined the concordance between the ATAC-seq signal intensity at accessible distal CREs in control and GLI1 OE cardiac progenitors *in vitro* and embryonic pSHF and HT *in vivo*. Pearson correlation analyses indicated increased similarity between pSHF and ESC-derived cardiac progenitor CRE accessibility profiles upon GLI1 OE (Fig. 3f). Conversely, the correlation between HT and ESC-derived cardiac progenitors decreased due to expression of GLI1 (Fig. 3f). These observations indicate that GLI^A promotes cardiac progenitor-specific chromatin accessibility at distal CREs, a potential mechanism for maintaining progenitor-specific gene expression of Hh target genes.

We hypothesized that the transition from GLI^A to GLI^R dominance during differentiation functioned as a molecular switch at distal progenitor-specific CREs to turn off progenitor-specific gene expression. We previously identified a GLI-bound distal

CRE upstream of the SHF Hh target gene *Foxf1*[16]. This enhancer dives SHF-specific reporter expression but is silenced in the heart *in vivo*, and therefore represents a progenitor-specific CRE and candidate for GLI^A (pSHF) to GLI^R (HT) transitional switch. The CRE contains 3 GLI-binding sites and binding sites for other cardiac TFs including 3 for TBX5[16]. TBX5 activated reporter expression from the CRE *in vitro* using a luciferase transcriptional reporter assay in HEK 293T cells (Fig. 4b). Co-transfection of GLI1 with TBX5 dramatically enhanced transcriptional activation (Fig. 4b). Conversely, co-transfection of $GLI3^R$ with TBX5 silenced TBX5-dependent transcriptional activity (Figure 4B). These results suggested that the ratio of GLI^A to GLI^R TF abundance was a dominant predictor of CRE activity, establishing a functional high-to-low switch as cardiomyocytes differentiate. This hypothesis predicted that GLI binding site would be required for switching CRE expression from on in progenitors to off in the heart. The GLI-bound, Hh activated *Foxf1* CRE demonstrated SHF-specific activity *in vivo*[16]. In contrast, the CRE harboring mutation of the 3 GLI binding sites demonstrated ectopic reporter expression in the HT (5/5 embryos with HT expression, Fig. 4c and Extended Data Fig. 6a-b). These results indicate that GLI-dependent CREs comprise a progenitor-on/cardiomyocyte-off molecular switch near progenitor-specific genes, providing a model for executing GLI^A/GLI^R TF abundance into cardiac progenitor-specific gene expression. This model suggests that maintenance of cardiac progenitor-specific gene expression in the pSHF requires dynamic activation of gene expression by GLI^A and subsequent repression by GLI^R as cells enter the inactive Hh signaling environment of the HT, implicating GLI TFs as a biphasic switch determining the timing of cardiac progenitor differentiation (Fig. 4d).

We elucidate a GLI TF-dependent switch controlling the maintenance of cardiac progenitor status. The transition from GLI^A to GLI^R experienced by cells migrating from the pSHF to the HT allows for the coordination of cardiac morphogenesis and cellular differentiation. These studies link the spatial distribution of signal-dependent TFs during embryonic development to the temporal regulation of a progenitor gene expression program. Hh-dependent maintenance of progenitor gene expression in the SHF allows for normal SHF morphogenesis, while a decrement of Hh signaling resulted in precocious differentiation and CHD. A strong association between cilia genes, required for Hh signaling, and CHD has recently been reported[30,31], suggesting that inappropriate differentiation control may play a significant role in CHD. Active Hh signaling in the SHF, causing delayed differentiation, provides a plausible mechanism explaining a key distinction between the early-differentiating FHF and the later-differentiating SHF.

Recent work has illuminated a role for Hh signaling in the maintenance of the stem cell niche important for repair and regeneration of several adult tissues. Hh signaling functions to maintain or expand quiescent stem cell populations in the regenerating hair follicle[5,32], intestinal enteroblasts[33], bladder epithelial cells[34], adult lung epithelium[35], skin[36] and brain[37-38]. Additionally, GLI TFs pattern the embryonic ventral neural tube by activating repressive TFs that prevent the acquisition of alternate fates[39]. Our results suggest that developmental patterning in multiple contexts may be controlled in part by Hh-dependent direct GLI^A TF activation of progenitor-specific networks, maintaining progenitor status and pausing differentiation until the Hh source is deprecated. Our results, in the context of these reports, suggest a possible role for Hh

signaling in the maintenance of progenitor populations and inhibition of differentiation across multiple tissue types during development and adult tissue homeostasis.

References

1. Petersen PH, Zou K, Krauss S, Zhong W. Continuing role for mouse Numb and Numbl in maintaining progenitor cells during cortical neurogenesis. *Nat Neurosci*. **8**, 803-11 (2004).

2. Wong YH, Lu AC, Wang YC, Cheng HC, Chang C, Chen PH, Yu JY, Fann MJ. Protogenin defines a transition stage during embryonic neurogenesis and prevents precocious neuronal differentiation. *J Neurosci*. **30**, 4428-39 (2010).

3. Vithayathil J, Pucilowska J, Goodnough LH, Atit RP, Landreth GE. Dentate Gyrus Development Requires ERK Activity to Maintain Progenitor Population and MAPK Pathway Feedback Regulation. *J Neurosci*. **35**, 6836-48 (2015).

4. Morrison SJ, Spradling AC. Stem cells and niches: mechanisms that promote stem cell maintenance throughout life. *Cell* **132**, 598-611 (2008).

5. Hsu YC, Li L, Fuchs E. Transit-amplifying cells orchestrate stem cell activity and tissue regeneration. *Cell* **157**, 935-49 (2014).

6. Zhou W, He Q, Zhang C, He X, Cui Z, Liu F, Li W. BLOS2 negatively regulates Notch signaling during neural and hematopoietic stem and progenitor cell development. *Elife* **5**. pii: e18108 (2016).

7. Volckaert T, Yuan T, Chao CM, Bell H, Sitaula A, Szimmtenings L, El Agha E, Chanda D, Majka S, Bellusci S, Thannickal VJ, Fässler R, De Langhe SP. Fgf10-Hippo Epithelial-Mesenchymal Crosstalk Maintains and Recruits Lung Basal Stem Cells. *Dev Cell* **43**, 48-59 (2017).

8. Garcia TX, Parekh P, Gandhi P, Sinha K, Hofmann MC. The NOTCH Ligand JAG1 Regulates GDNF Expression in Sertoli Cells. *Stem Cells Dev*. **26**, 585-598 (2017).

9. Briscoe J, Thérond PP. The mechanisms of Hedgehog signalling and its roles in development and disease. *Nat Rev Mol Cell Biol.* **14**, 416-29 (2013).

10. Petrova R, Joyner AL. Roles for Hedgehog signaling in adult organ homeostasis and repair. *Development* **141**, 3445-57 (2014).

11. Merchant AA, Matsui W. Targeting Hedgehog--a cancer stem cell pathway. *Clin Cancer Res* **16**, 3130-40 (2010).

12. Cochrane CR, Szczepny A, Watkins DN, Cain JE. Hedgehog Signaling in the Maintenance of Cancer Stem Cells. *Cancers (Basel)* **7**, 1554-85 (2015).

13. Kelly RG. The second heart field. *Curr Top Dev Biol* **100**, 33-65 (2012).

14. Goddeeris, M. M. *et al.* Intracardiac septation requires hedgehog-dependent cellular contributions from outside the heart. *Development* **135,** 1887–1895 (2008).

15. Hoffmann, A. D., Peterson, M. A., Friedland-Little, J. M., Anderson, S. A. & Moskowitz, I. P. sonic hedgehog is required in pulmonary endoderm for atrial septation. *Development* **136**, 1761–1770 (2009).

16. Hoffmann, A. D. *et al.* PLOS Genetics: Foxf Genes Integrate Tbx5 and Hedgehog Pathways in the Second Heart Field for Cardiac Septation. *journals.plos.org* 10, e1004604 (2014).

17. Izraeli S, Lowe LA, Bertness VL, Good DJ, Dorward DW, Kirsch IR, Kuehn MR. The SIL gene is required for mouse embryonic axial development and left-right specification. *Nature* **399**, 691-4 (1999).

18. Kim PC, Mo R, Hui Cc C. Murine models of VACTERL syndrome: Role of sonic hedgehog signaling pathway. *J Pediatr Surg.* **36**, 381-4 (2001).

19. Meyers EN, Martin GR. Differences in left-right axis pathways in mouse and chick: functions of FGF8 and SHH. *Science* **285**, 403-6 (1999).

20. Tsukui T, Capdevila J, Tamura K, Ruiz-Lozano P, Rodriguez-Esteban C, Yonei-Tamura S, Magallón J, Chandraratna RA, Chien K, Blumberg B, Evans RM, Belmonte JC. Multiple left-right asymmetry defects in Shh(-/-) mutant mice unveil a convergence of the shh and retinoic acid pathways in the control of Lefty-1. *Proc Natl Acad Sci U S A*. **96**, 11376-81 (1999).

21. Vokes SA, Ji H, Wong WH, McMahon AP. A genome-scale analysis of the cis-regulatory circuitry underlying sonic hedgehog-mediated patterning of the mammalian limb. *Genes Dev*. **22**, 2651-63 (2008).

22. Mugford, J. W., Sipilae, P., McMahon, J. A. & McMahon, A. P. Osr1 expression demarcates a multi-potent population of intermediate mesoderm that undergoes progressive restriction to an Osr1-dependent nephron progenitor compartment within the mammalian kidney. *Developmental Biology* **324**, 88–98 (2008).

23. Kattman SJ, Witty AD, Gagliardi M, Dubois NC, Niapour M, Hotta A, Ellis J, Keller G. Stage-specific optimization of activin/nodal and BMP signaling promotes cardiac differentiation of mouse and human pluripotent stem cell lines. *Cell Stem Cell* **8**, 228-40 (2011).

24. Dai P, Akimaru H, Tanaka Y, Maekawa T, Nakafuku M, Ishii S. Sonic Hedgehog-induced activation of the Gli1 promoter is mediated by GLI3. *J Biol Chem*. **274**, 8143-52 (1999).

25. Agren M, Kogerman P, Kleman MI, Wessling M, Toftgård R. Expression of the PTCH1 tumor suppressor gene is regulated by alternative promoters and a single functional Gli-binding site. *Gene* **330**, 101-14 (2004).

26. Vokes SA, Ji H, McCuine S, Tenzen T, Giles S, Zhong S, Longabaugh WJ, Davidson EH, Wong WH, McMahon AP. Genomic characterization of Gli-activator targets in sonic hedgehog-mediated neural patterning. *Development* **134**, 1977-89 (2007).

27. Buenrostro JD, Giresi PG, Zaba LC, Chang HY, Greenleaf WJ. Transposition of native chromatin for fast and sensitive epigenomic profiling of open chromatin, DNA-binding proteins and nucleosome position. *Nat Methods* **10**, 1213-8 (2013).

28. Palmer CJ, Galan-Caridad JM, Weisberg SP, Lei L, Esquilin JM, Croft GF, Wainwright B, Canoll P, Owens DM, Reizis B. Zfx facilitates tumorigenesis caused by activation of the Hedgehog pathway. *Cancer Res.* **74**, 5914-24 (2014).

29. Briggs KJ, Corcoran-Schwartz IM, Zhang W, Harcke T, Devereux WL, Baylin SB, Eberhart CG, Watkins DN. Cooperation between the Hic1 and Ptch1 tumor suppressors in medulloblastoma. *Genes Dev*. **22**, 770-85 (2008).

30. Li Y, Klena NT, Gabriel GC, Liu X, Kim AJ, Lemke K, Chen Y, Chatterjee B, Devine W, Damerla RR, Chang C, Yagi H, San Agustin JT, Thahir M, Anderton S, Lawhead C, Vescovi A, Pratt H, Morgan J, Haynes L, Smith CL, Eppig JT, Reinholdt L, Francis R, Leatherbury L, Ganapathiraju MK, Tobita K, Pazour GJ, Lo CW. Global genetic analysis in mice unveils central role for cilia in congenital heart disease. *Nature* **521**, 520-4 (2015).

31. Burnicka-Turek O, Steimle JD, Huang W, Felker L, Kamp A, Kweon J, Peterson M, Reeves RH, Maslen CL, Gruber PJ, Yang XH, Shendure J, Moskowitz IP. Cilia gene mutations cause atrioventricular septal defects by multiple mechanisms. *Hum Mol Genet.* **25**, 3011-3028 (2016).

32. Ouspenskaia T, Matos I, Mertz AF, Fiore VF, Fuchs E. WNT-SHH Antagonism Specifies and Expands Stem Cells prior to Niche Formation. *Cell* **164**, 156-169 (2016).

33. Tian A, Shi Q, Jiang A, Li S, Wang B, Jiang J. Injury-stimulated Hedgehog signaling promotes regenerative proliferation of Drosophila intestinal stem cells. *J Cell Biol*. **208**, 807-19 (2015).

34. Shin K, Lee J, Guo N, Kim J, Lim A, Qu L, Mysorekar IU, Beachy PA Hedgehog/Wnt feedback supports regenerative proliferation of epithelial stem cells in bladder. *Nature* **472**, 110-4 (2011).

35. Peng, T. *et al.* Hedgehog actively maintains adult lung quiescence and regulates repair and regeneration. *Nature* **526**, 578–582 (2015).

36. Sen GL, Reuter JA, Webster DE, Zhu L, Khavari PA. DNMT1 maintains progenitor function in self-renewing somatic tissue. *Nature* **463**, 563-7 (2010).

37. Ahn S, Joyner AL. In vivo analysis of quiescent adult neural stem cells responding to Sonic hedgehog. *Nature* **437**, 894-7 (2005).

38. Wojcinski A, Lawton AK, Bayin NS, Lao Z, Stephen DN, Joyner AL. Cerebellar granule cell replenishment postinjury by adaptive reprogramming of Nestin^{+} progenitors. *Nat Neurosci* **20**, 1361-1370 (2017).

39. Kutejova E, Sasai N, Shah A, Gouti M, Briscoe J. Neural Progenitors Adopt Specific Identities by Directly Repressing All Alternative Progenitor Transcriptional Programs. *Dev Cell* **36**, 639-53 (2016).

40. Huang da W, Sherman BT, Lempicki RA. Systematic and integrative analysis of large gene lists using DAVID bioinformatics resources. *Nat Protoc*. **4**, 44-57 (2009).

41. Schneider CA, Rasband WS, Eliceiri KW. NIH Image to ImageJ: 25 years of image analysis. *Nat Methods* **9**, 671-5 (2012).

42. Iacovino M, Bosnakovski D, Fey H, Rux D, Bajwa G, Mahen E, Mitanoska A, Xu Z, Kyba M. Inducible cassette exchange: a rapid and efficient system enabling conditional gene expression in embryonic stem and primary cells. *Stem Cells* **29**, 1580-8 (2011).

43. Andrews S. (2010). FastQC: a quality control tool for high throughput sequence data. Available online at: http://www.bioinformatics.babraham.ac.uk/projects/fastqc

44. Langmead B, Salzberg SL. Fast gapped-read alignment with Bowtie 2. *Nat Methods* **9**, 357-9 (2012).

45. Trapnell C, Williams BA, Pertea G, Mortazavi A, Kwan G, van Baren MJ, Salzberg SL, Wold BJ, Pachter L. Transcript assembly and quantification by RNA-Seq reveals unannotated transcripts and isoform switching during cell differentiation. *Nat Biotechnol.* **28**, 511-5 (2010).

46. Robinson MD, McCarthy DJ, Smyth GK. edgeR: a Bioconductor package for differential expression analysis of digital gene expression data. *Bioinformatics* **26**, 139-40 (2010).

47. Zhang Y, Liu T, Meyer CA, Eeckhoute J, Johnson DS, Bernstein BE, Nusbaum C, Myers RM, Brown M, Li W, Liu XS. Model-based analysis of ChIP-Seq (MACS). *Genome Biol*. **9**, R137 (2008).

48. Quinlan AR, Hall IM. BEDTools: a flexible suite of utilities for comparing genomic features. *Bioinformatics* **26**, 841-2 (2010).

49. Timothy L. Bailey, Mikael Bodén, Fabian A. Buske, Martin Frith, Charles E. Grant, Luca Clementi, Jingyuan Ren, Wilfred W. Li, William S. Noble. MEME SUITE: tools for motif discovery and searching. *Nucleic Acids Research* **37**, W202-W208 (2009).

50. H. Wickham. ggplot2: elegant graphics for data analysis. Springer New York, 2009.

51. Kothary R, Clapoff S, Darling S, Perry MD, Moran LA, Rossant J. Inducible expression of an hsp68-lacZ hybrid gene in transgenic mice. *Development* **105**, 707-14 (1989).

Methods

Animal Husbandry

Mouse experiments were completed according to a protocol reviewed and approved by the Institutional Animal Care and Use Committee of the University of Chicago, in compliance with the USA Public Health Service Policy on Humane Care and Use of Laboratory Animals. The *Shh*$^{-/-}$ mouse line was obtained from the Jackson laboratory. CD1 embryos were obtained from Charles River Laboratories. *Osr1*$^{eGFPCre\text{-}ERt2}$(22) and *ROSA26*$^{Gli3T\text{-}Flag}$(21) lines were reported previously.

Embryo transcriptome profiling

The pSHF was microdissected from five individual E10.5 *Shh*$^{+/+}$ and five *Shh*$^{-/-}$ embryos, and yolk sacs were collected for genotyping. Tissues were mechanically homogenized in TRIzol Reagent (ThermoFisher Scientific 15596026), and RNA was isolated using RNeasy Mini RNA Isolation Kit (Qiagen 74104). Overall, 12µg of total RNA for each sample was treated with the mouse GLOBINclear kit (ThermoFisher Scientific AM1980) to remove the majority of globin RNA. 1ug of total RNA was then used to generate sequencing libraries using the TruSeq RNA Sample prep kit v2 (Illumina RS-122-2001), as per recommended instructions. Libraries were quantitated on an Agilent Bio-Analyzer and pooled in equimolar amounts. Pooled libraries were sequenced on the HiSeq2500 in Rapid Run Mode following the manufacturer's protocols to generate stranded single-end reads of 50bp. The number of sequenced reads per sample ranged between 11.7 million 17.7 million with an average of 15 million sequenced per sample. Quality control for raw reads involved trimming the first 13bp with FastQ Groomer to ensure a median

quality score of 36 or above for each sample. Fastq files were aligned to the UCSC mouse genome (mm9) using TopHat (version 2.0.10) with the following parameters: (--segment-length 19 --segment-mismatches 2 --no-coverage-search). Between 11.4 million 17.2 million successfully mapped reads were then merged. One $Shh^{+/+}$ sample was discarded due to discordance with all other samples. Remaining samples were then analyzed for differential gene expression using Cuffdiff (version 2.1.1) with quartile normalization. Significantly differentially expressed genes were identified using thresholds of FDR <0.05 and fold change > 1.5, resulting in 204 and 52 genes up-regulated and down-regulated, respectively, in the $Shh^{-/-}$ pSHF samples compared with $Shh^{+/+}$ samples.

The pSHF and HT from six CD1 embryos was also microdissected and RNA-seq analysis was performed to identify genes differentially expressed between the two tissues. $Shh^{-/-}$ dysregulated genes were then plotted on top of pSHF vs HT differentially expressed genes using R, and the distributions of $Shh^{-/-}$ downregulated and $Shh^{-/-}$ upregulated genes were compared to the distribution of all genes using Welch's two-sample T-test. Differential expression of selected genes identified by RNA-seq was validated using qPCR. RNA was harvested from $Shh^{+/+}$ and $Shh^{-/-}$ pSHF samples with a Nucleospin RNA extraction kit (Machery-Nagel 740955.250). RNA was then used to perform one-step qPCR with the iTaq One-Step system (Bio-Rad 1725151), and expression levels in mutant samples were normalized to $Shh^{+/+}$ samples. RNA-seq identified differentially expressed genes were also used to identify associated gene ontology (GO) terms that were enriched above a *P*-value cutoff of 0.05 using the DAVID 6.8 Functional Annotation tool[40].

Embryo Immunohistochemistry / Immunofluorescence

E10.5 embryos were harvested from timed pregnancies and yolk sacs were collected for genotyping. Embryos were fixed overnight in 4% paraformaldehyde, washed with PBS and processed for paraffin sectioning. 5um serial sections were generated and used for immunofluorescence with primary antibodies recognizing sarcomeric myosin (1:20; DSHB MF20) and Alexa Fluor-conjugated secondary antibodies (1:1000; ThermoFisher Scientific). Antigen retrieval was performed on all sections with 10mM sodium citrate buffer. DAPI was used to counterstain tissues and provide a tissue reference. Sections were imaged with an Olympus IX81 inverted widefield microscope using 10x and 20x objectives in the University of Chicago's Integrated Light Microscopy Core Facility. Images were processed with ImageJ[41].

Histology

Activation of *CreER*^{T2} was accomplished by intraperitoneal injection with 2 mg tamoxifen (TM) per dose in corn oil to pregnant dams, as previously described[15]. Pregnant *ROSA26*$^{Gli3T\text{-}Flag\ c/c}$ females were dosed at E7.5, E8.5 and E9.5, and histological studies were performed at E14.5. Embryos were harvested and fixed in 4% paraformaldehyde overnight at 4ºC, and then processed for paraffin sectioning. 5um sections were then stained with hematoxylin and eosin to reveal the structural morphology of the atrial septum in mutant and control embryos.

mESC line generation and differentiation culture

To generate an inducible GLI1 mouse embryonic stem cell (mESC) line, the coding sequence for mouse *Gli1* was inserted into the *Hprt* locus of A2Lox.cre mES cells using a method previously described[42]. Individual clones were assessed for differentiation potential and doxycycline-inducibility (data not shown). One clone was chosen and used for all experiments described herein, and all experiments were performed at the same passage number. mESCs were maintained and differentiated into cardiomyocytes as previously described[23].

For GLI1 overexpression experiments, doxycycline (Sigma D9891) was added to cultures at the cardiac progenitor stage (Day 5). Cells were then washed and media was changed after 24hrs of exposure to doxycycline. qPCR and western blots were performed, as described above, on Day 6 samples to assess the expression level of *Gli1* and Hh targets, relative to untreated controls. Expression of the Hh target, *Foxf1*, was quantified relative to *Gapdh* expression in cells treated with increasing concentrations of doxycycline and relative to *Gapdh* in pSHF embryo samples. Based on results from these assays, a final doxycycline concentration of 500ng/ml was chosen for all GLI1 overexpression experiments.

mESC immunofluorescence was performed, as above, with an antibody recognizing cardiac Troponin T (1:100; ThermoFisher Scientific MS-295-P1). The area of cTnT positivity was calculated as the average area / mm^2 of 5 fields of view across two biological replicates per condition, using the threshold measurement tool in ImageJ. The number of beating foci was calculated as the average number of independently beating regions within 5 fields of view across two biological samples, counted from 5 second videos taken on a Zeiss Axiovert 200m inverted widefield microscope. RNA-seq

was performed on at least two replicate Day 6, Day 8 and Day 12 GLI1 OE and control samples. Data were analyzed with FastQC[43], reads were mapped to the mouse genome (mm9) with Bowtie2[44] and transcripts were assigned and quantified with Cufflinks with default parameters[45]. Reads were then normalized and differentially expressed genes for each timepoint were identified with edgeR[46]. Differentially expressed genes were then filtered to include only genes with a fold change ≥ 0.5 (log^2) and an FDR ≤ 0.05. GO term analysis on Day 6 dysregulated genes, and qPCR validation of selected genes, was performed as described above. The mean log2 fold changes of downregulated, upregulated and all genes were compared with a non-parametric Kruskall-Wallis rank sum test for Day 6, Day 8 and Day 12 samples: Day 6 chi-squared = 3804.9, df = 2, p-value < $2.2e^{-16}$; Day 8 chi-squared = 397.45, df = 2, p-value < $2.2e^{-16}$; Day 12 chi-squared = 363.78, df = 2, p-value < $2.2e^{-16}$.

Chromatin profiling

Assay for transposase-accessible chromatin was performed as previously described[27]. Briefly, the pSHF and HT were microdissected from CD1 embryos, pooled into three replicates, and dissociated with TrypLE (ThermoFisher Scientific 12605-010). For mESC samples, 150,000 cells were collected from two replicate GLI1 OE and control samples. Embryo and cell samples were then lysed, as described[27], and transposition was carried out at 37C for 30 minutes with Illumina's Nextera DNA Library Prep kit (Illumina 15028212). Libraries were generated from transposed DNA and sequenced on an Illumina HiSeq4000 instrument in the University of Chicago's Genomic Facility. Data

were analyzed with FastQC and mapped to the mouse genome (mm9) with Bowtie2 using default parameters. Peaks were called for all samples with MACS2[47] using the following parameters: -q 0.05 --nomodel --shift -100 --extsize 200 --nolambda --keep-dup all --call-summits... Peak sets from biological replicates were overlapped with the Bedtools[48] intersect tool to identify replicated peaks. Peaks sets generated from regions present in both replicates were then intersected to identify regions specific to each tissue type. For motif analysis, the summits from replicated regions were extended ±250bp, and sequence was retrieved for these regions. *De novo* and targeted motif (GLI and GLI-similar) enrichment analysis was then performed using the MEME Suite of tools[49] with a randomized or shuffled background. Pearson's correlation was calculated for read enrichment within region subsets in R and data were visualized with ggplot2[50]. To compare GLI1 OE-specific accessible chromatin regions to embryonic pSHF accessible regions, a Monte Carlo simulation was run. The number of overlapping GLI1 OE-specific and pSHF-specific regions was determined. Next, the combined embryonic regions (pSHF + HT) were used as the background from which 1000 random samplings were taken. These samplings were then overlapped with GLI1 OE-specific regions, and the *P*-value was calculated as: *P* = (# overlaps simulated > overlaps observed) + 1 / number of simulations + 1.

Luciferase Assays

Expression vectors for mouse *Gli1*, *Gli3T* and *Tbx5*, as well as a luciferase vector containing the *Foxf1* enhancer were previously described[16]. Expression and reporter vectors were transfected into HEK293T cells using FuGENE HD (Promega E2311).

Cells were cultured for 48 hours after transfection, then lysed and assayed using a Dual-Luciferase Reporter Assay system (Promega E1960).

Transient transgenics

The *Foxf1a* enhancer and minimal promoter used in the luciferase assays were subcloned from the pENTR vector into the Hsp68-LacZ vector[51] using the Gateway system (Invitrogen). GLI binding sites were mutated using the Agilent QuikChange Multi site-directed mutagenesis kit (Agilent 210515-5). The resulting constructs were digested with NotI enzyme to remove the pBlueScript backbone, gel-purified, injected into fertilized mouse eggs at the University of Chicago Transgenics Core Facility and implanted into female mice. Five embryos were harvested at E9.5 and stained as described previously[15].

Author contributions

M.R. designed and performed the experiments and wrote the manuscript. A.D.H., J.D.S., A.G., S.L., N.D., E.L. and J.J-L. performed *in vivo* experiments. C.K., S.Y., E.H., and E.L. performed *in vitro* experiments. X.H.Y., C.P-C. and K.I. performed computational analyses. S.S-K.C. and M.K. generated the GLI1-FTA mESC line. D.J.G. designed the experiments. I.P.M. designed the experiments and wrote the manuscript.

Competing Interests

The authors report no competing interests.

Figures

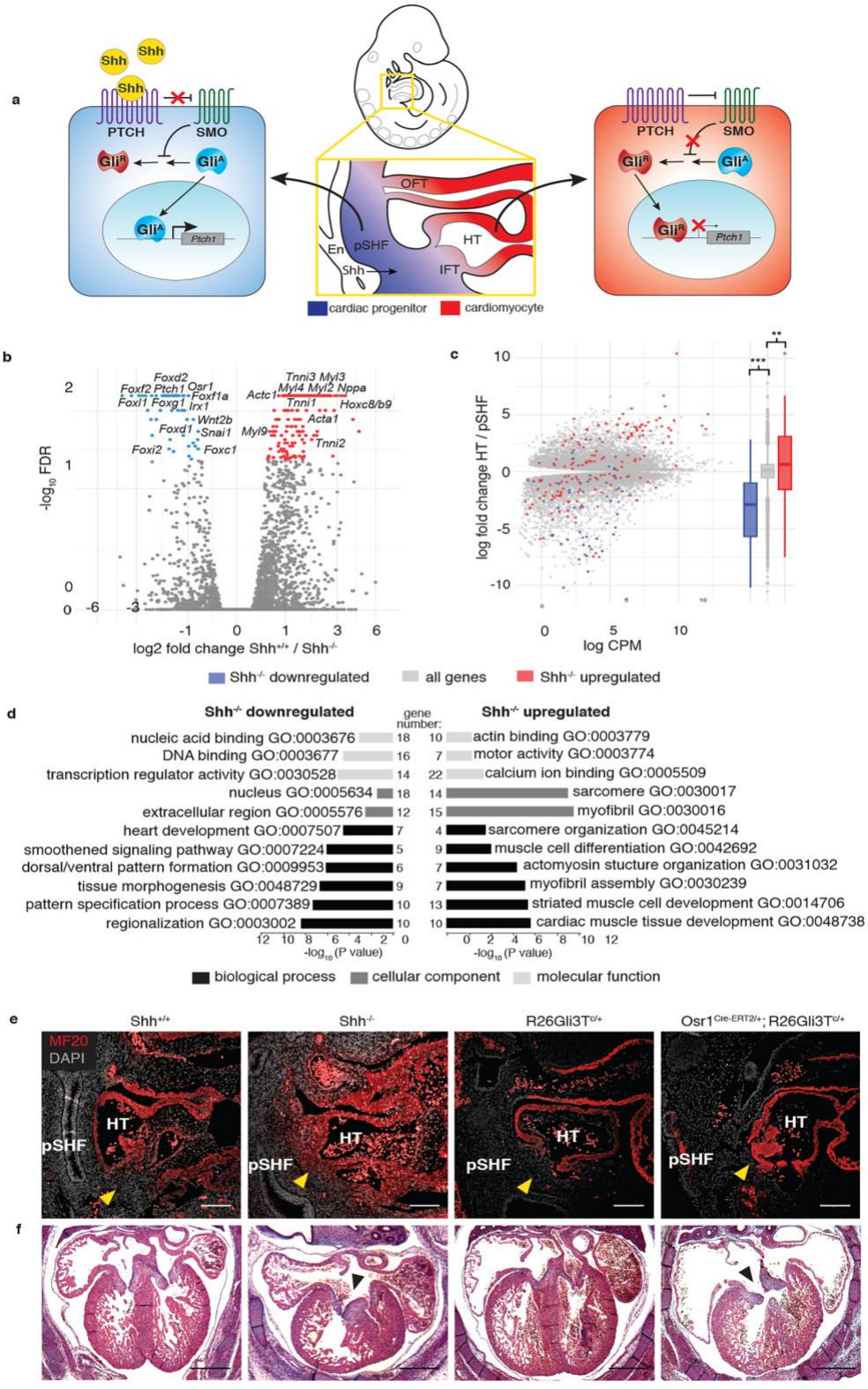

Figure 1. Hedgehog signaling activates a progenitor-specific gene regulatory network in the pSHF. a, Schematic of cardiac progenitors (blue) in the E10.5 pSHF and differentiating cardiomyocytes (red) in the HT, sagittal view. Active Hh signaling in the pSHF leads to accumulation of GLI^A in the nucleus and the activation of Hh target genes, such as *Ptch1* (left). Inactive Hh signaling results in the truncation of GLI^A to GLI^R and accumulation of the repressor in the nucleus (right). **b**, Volcano plot displaying upregulated and downregulated genes in the $Shh^{-/-}$ pSHF. Red is upregulated, blue is downregulated. **c**, MA plot and box plots illustrating the distribution of $Shh^{-/-}$ downregulated and upregulated genes in the wild type pSHF and HT. Welch's T-test on downregulated vs all genes *P*-value = $1.05x10^{8}$; upregulated vs all genes *P*-value = 0.02. **d**, Gene ontology (GO) analysis of $Shh^{-/-}$ dysregulated genes. **e**. Immunofluorescent staining for MF20 (sarcomeric myosin) in the E10.5 pSHF of control and Hh mutant embryos (grey = DAPI, red = MF20). **f**. Histological sections of E14.5 hearts from control and Hh mutant embryos. Scale bars in **e**, **f** = 200um.

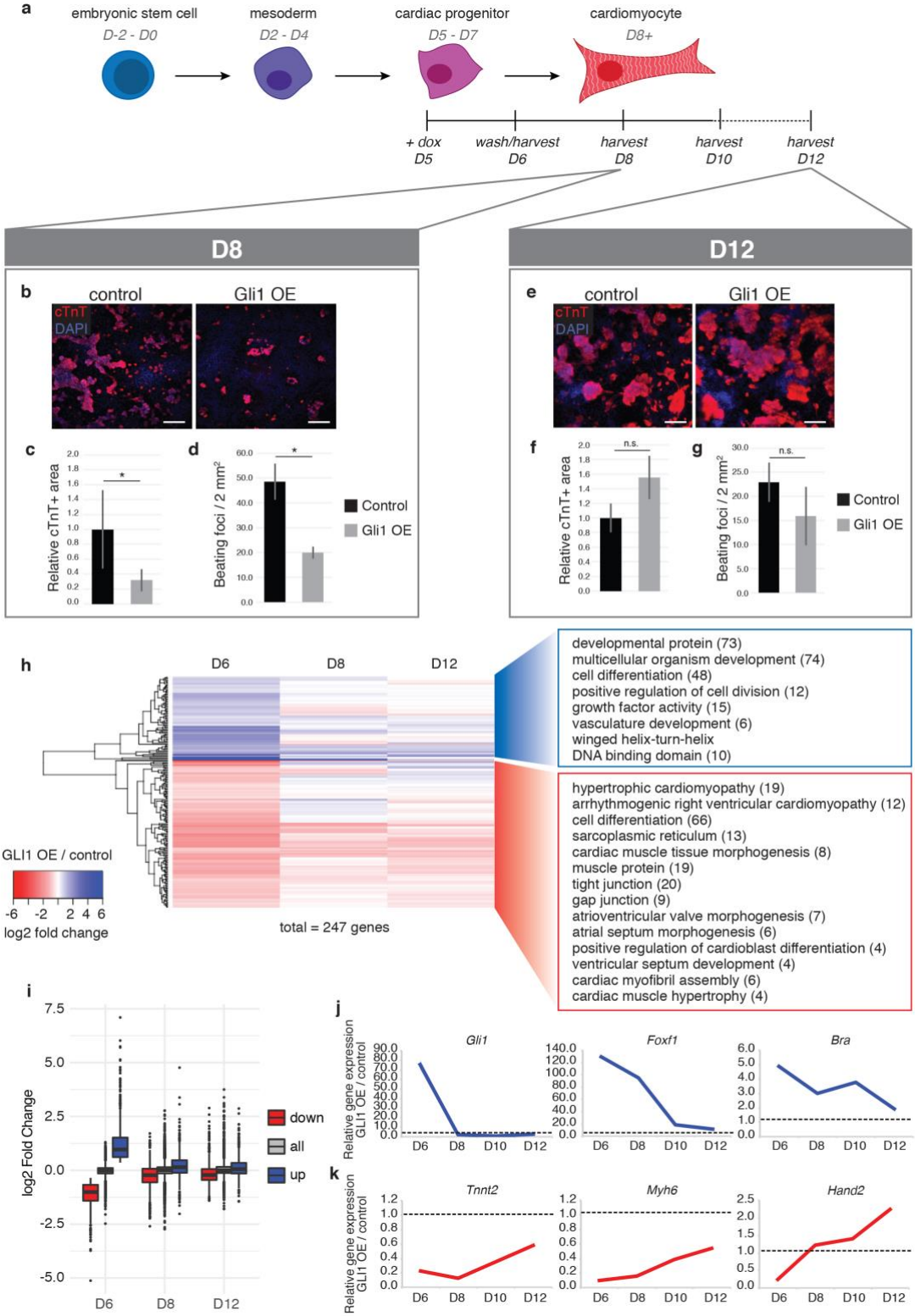

Figure 2. GLI^{A} expression in cardiac progenitors delays cardiomyocyte differentiation. a, Schematic of the *in vitro* cardiomyocyte differentiation system and GLI1 OE experimental design. **b**, Immunofluorescent staining for cardiac troponin (cTnT) in control and GLI1 OE cells harvested at Day 8. **c**, Quantification of the area of cTnT-positivity in control and GLI1 OE cells at Day 8. **d**, Quantification of the number of beating foci in videos taken of control and GLI1 OE cells at Day 8. **e**, Immunofluorescent staining for cardiac troponin in control and GLI1 OE cells harvested at Day 12. **f**, Quantification of the area of cTnT-positivity in control and GLI1 OE cells at Day 12. **g**, Quantification of the number of beating foci in videos taken of control and GLI1 OE cells at Day 12. **h**, Differential gene expression time series and GO analyses of GLI1 OE cells. GO terms shown are those associated with development and differentiation from gene dysregulated at Day 6. **i**, Time series of the mean log2 fold change of genes downregulated and upregulated at Day 6, and their fold changes at Day 8 and Day 12, relative to all genes. **j.** qPCR validation of a temporary downregulation of progenitor-specific genes in GLI1 OE cells. **k**, qPCR validation of a temporary upregulation of cardiomyocyte-specific genes in GLI1 OE cells. Scale bars in **b**,**e** = 100um.

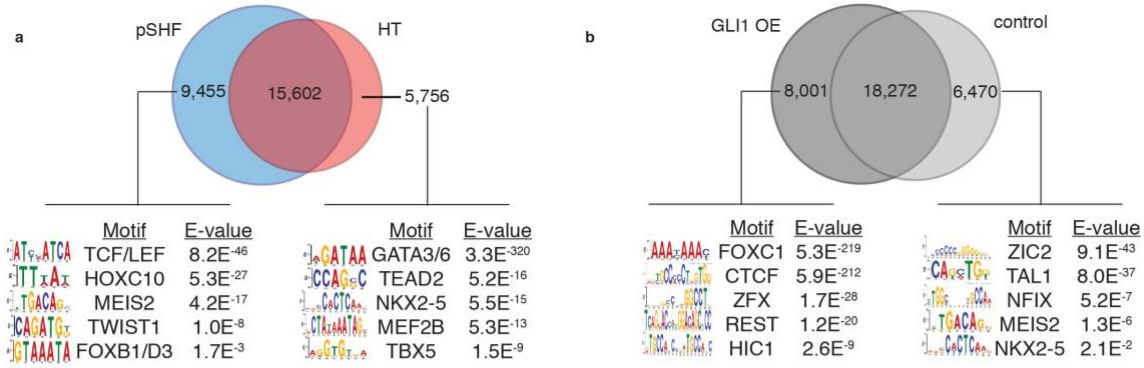

c

Motif Name	PWM ID	pSHF-specific	HT-specific	GLI1 OE CP-specific	control CP-specific
Hs GLI2	MA0734.1	*3.74E-20*	*not enriched*	*1.13E-22*	*not enriched*
Hs GLIS1	MA0735.1	*1.06E-50*	*not enriched*	*3.27E-05*	*not enriched*
HS GLIS2	MA0736.1	*2.42E-70*	*not enriched*	*not enriched*	*not enriched*
Hs GLIS3	MA0737.1	*3.75E-28*	*not enriched*	*3.83E-02*	*not enriched*
Mm GLIS2	PB0025.1	*1.09E-37*	*not enriched*	*not enriched*	*2.58E-02*
Hs TBX5	MA0807.1	*not enriched*	*1.88E-11*	*not enriched*	*not enriched*
Mm NKX2-5	MA0503.1	*not enriched*	*4.83E-14*	*not enriched*	*1.90E-05*
Mm GATA4	MA0482.1	*not enriched*	*1.01E-289*	*not enriched*	*6.30E-03*

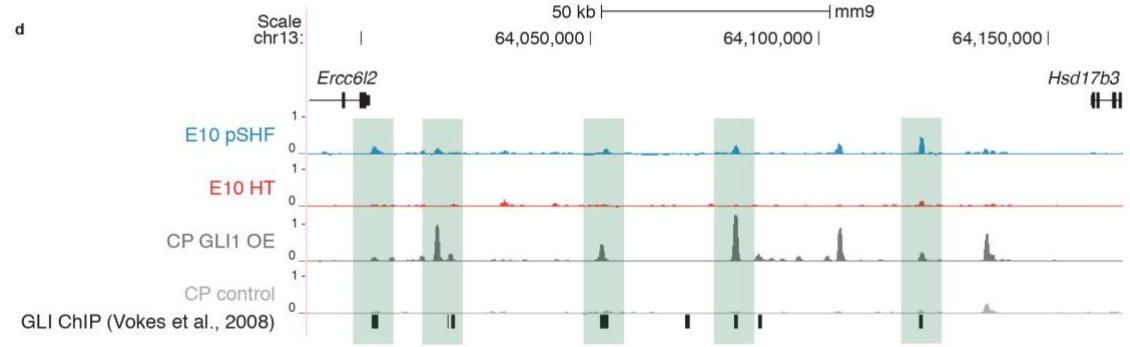

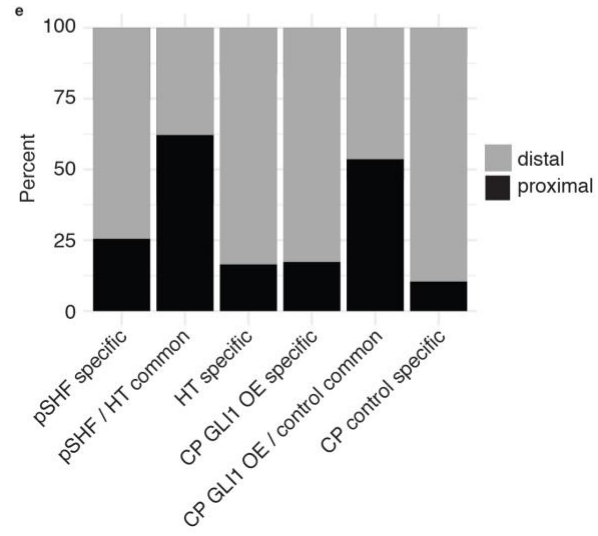

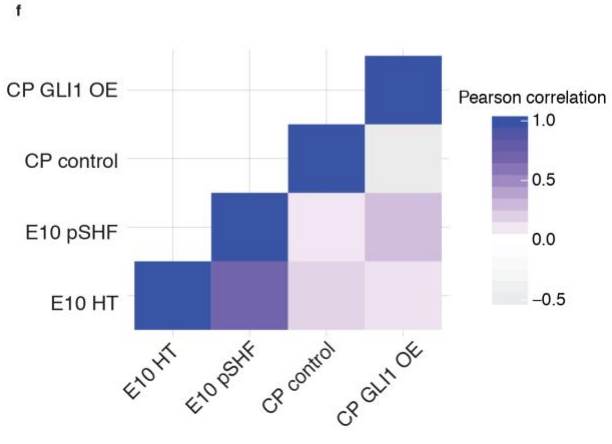

Figure 3. GLI^{A} expression remodels chromatin at distal CREs near progenitor-specific genes. a, Venn diagram showing common and specific accessible chromatin regions in the embryonic pSHF and HT, and TF motifs enriched in each subset. **b**, Venn diagram showing common and specific accessible chromatin regions in GLI1 OE cells and control cells, and TF motifs enriched in each subset. **c**, GLI consensus and GLI-similar (GLIS) binding motif enrichment in embryonic pSHF-specific and GLI1 OE-specific regions and cardiogenic TF binding motif enrichment in HT-specific and control cell-specific regions. **d**, ATAC-seq read enrichment and GLI ChIP-seq binding regions at a putative regulatory locus upstream of *Ptch1* in embryonic tissues and cardiac progenitor (CP) cells. **e**, Stacked bar graph depicting the location of accessible regions relative to the closest TSS of all tissue-specific peaks (proximal is ≤ 1.5kb; distal is ≥ 1.5kb). **f**. Correlation between pSHF and HT-specific distal chromatin profiles and GLI1 OE and control cell chromatin profiles.

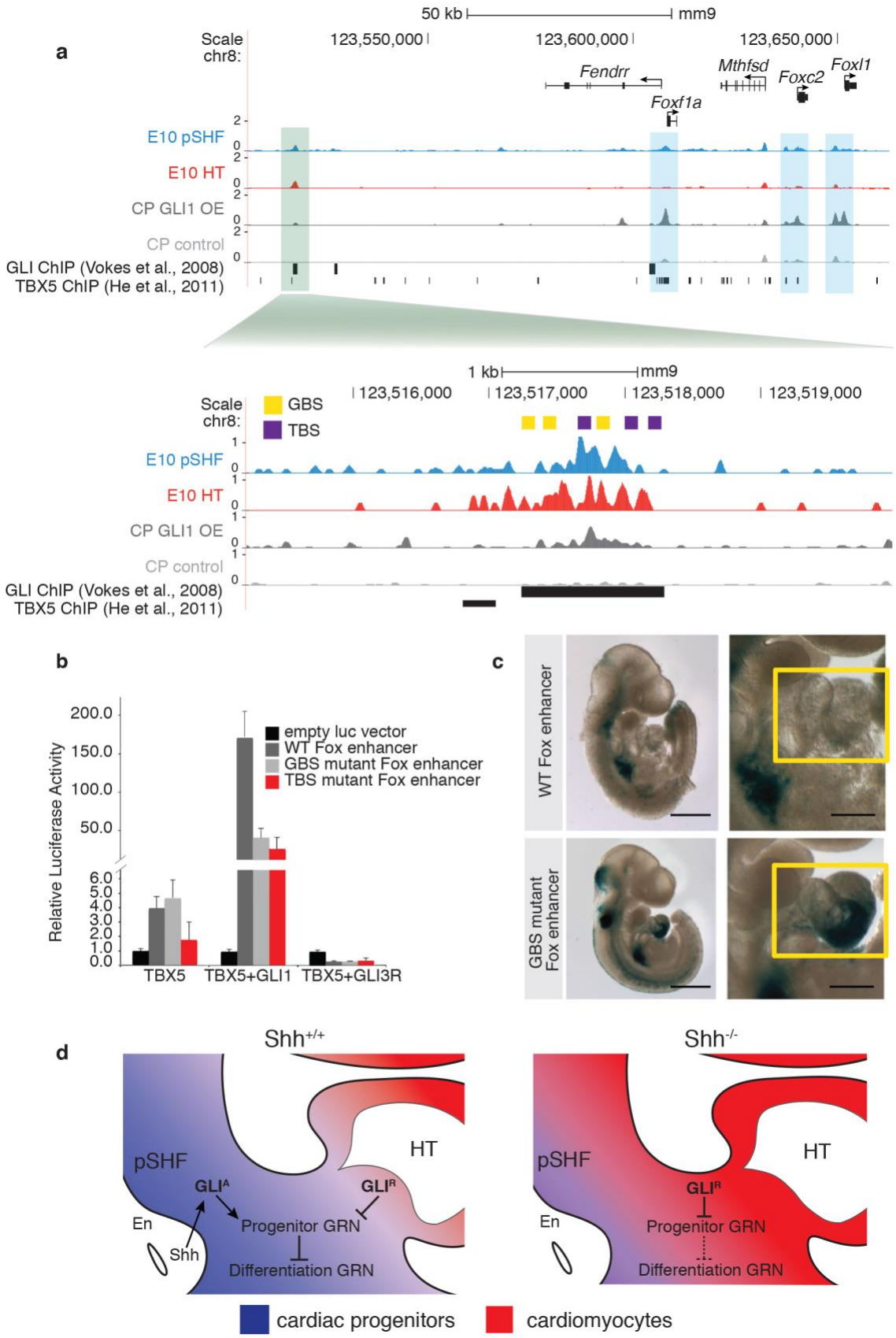

Figure 4. GLI transcription factors act as a biphasic switch on a progenitor-specific regulatory element located near Hh target genes. a, ATAC-seq read enrichment and GLI/TBX5 ChIP-seq peaks at a putative regulatory element upstream of the Hh-dependent *Foxf1* target in the pSHF, HT, GLI1 OE and control cardiac progenitor (CP) cells. GBS = GLI binding site; TBS = TBX5 binding site. **b**, Luciferase reporter activity modulated by GLI^A and GLI^R at the *Foxf1* enhancer, in cooperation with TBX5. Mutation of all three GLI binding sites (GBS) or TBX binding sites (TBS) did not completely abrogate reporter activation by GLI1 and TBX5, suggesting that their cooperation is not entirely dependent on direct DNA binding. **c**, Transient transgenic analysis of reporter expression driven by wild type and GBS mutant versions of the *Foxf1* CRE. **d**, Model depicting the Hh-dependent activation of a progenitor gene regulatory network in the embryonic pSHF by GLI^A and repression of the progenitor GRN in the HT by GLI^R. In Hh mutant embryos, the progenitor GRN is not activated and precocious differentiation of cardiomyocytes is permitted, resulting in severe cardiac defects. Scale bar in **c** (left) = 300um, **c** (right) = 100um.

Extended Data Figures

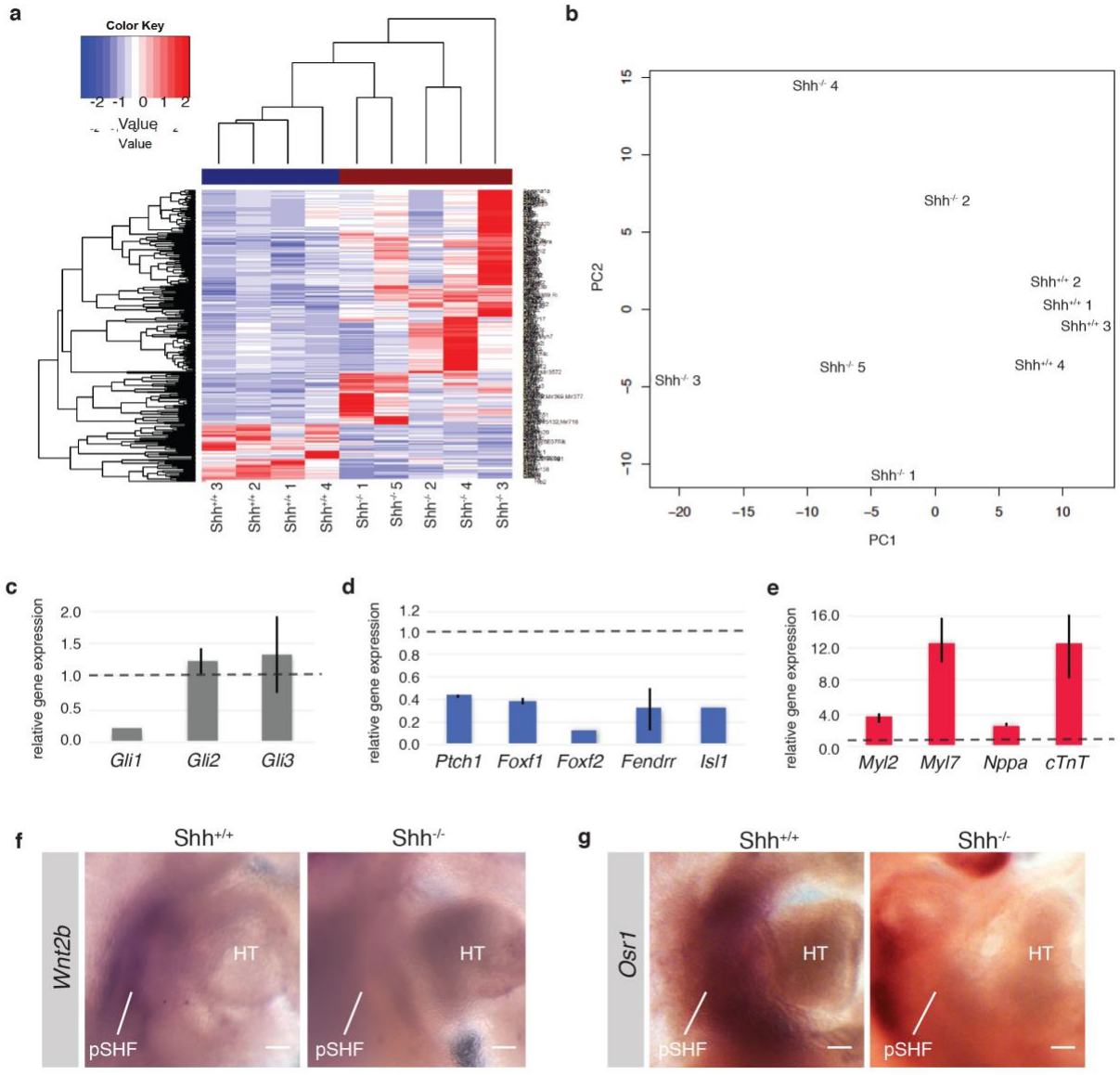

Extended Data Figure 1. Differential gene expression analysis reveals downregulation of progenitor genes expressed in the SHF. a, Heatmap showing differentially expressed genes in $Shh^{+/+}$ and $Shh^{-/-}$ replicate samples. **b**, PCA plot of differentially expressed genes demonstrating that genotype accounts for the highest proportion of variation among embryo gene expression profiles. **c**, qPCR validation of reduced Hh activation in the *Shh*$^{-/-}$ pSHF. **d**, qPCR validation of downregulated progenitor genes in the *Shh*$^{-/-}$ pSHF. **e**, qPCR validation of upregulated cardiomyocyte genes in the *Shh*$^{-/-}$ pSHF. **f**, *In situ* hybridization of *Wnt2b* in the SHF of *Shh*$^{+/+}$ and *Shh*$^{-/-}$ embryos demonstrating pSHF-specific loss of gene expression. **g**, *In situ* hybridization of *Osr1* in the SHF of *Shh*$^{+/+}$ and *Shh*$^{-/-}$ embryos demonstrating pSHF-specific loss of gene expression. Scale bar = 100um.

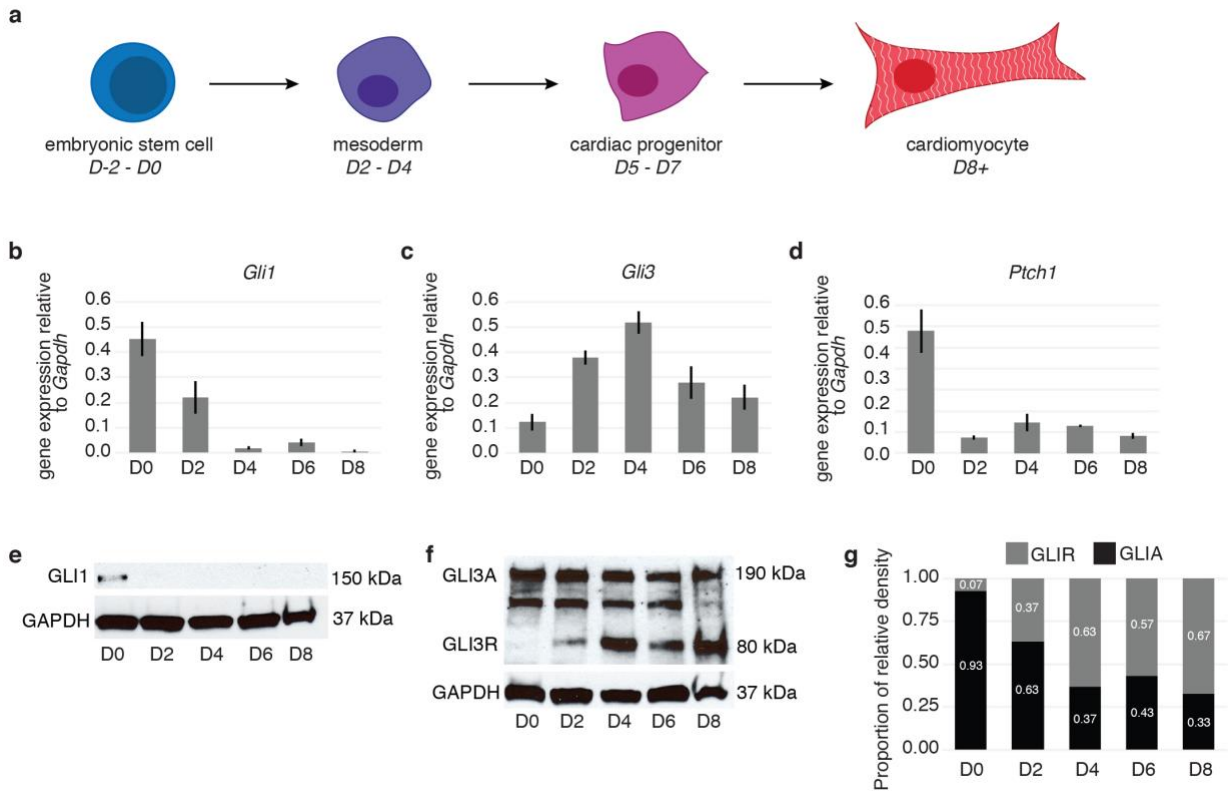

Extended Data Figure 2. Hedgehog signaling is inactive during mESC-derived cardiomyocyte differentiation. **a**, Schematic depicting the *in vitro* cardiomyocyte differentiation system employed in these studies. **b**, Expression level of *Gli1*, relative to *Gapdh*, during cardiomyocyte differentiation. **c**, Expression level of *Gli3*, relative to *Gapdh*, during cardiomyocyte differentiation. **d**, Expression level of the Hh target *Ptch1*, relative to *Gapdh*, during cardiomyocyte differentiation. **e**, Western blot demonstrating the expression level of GLI1 protein during cardiomyocyte differentiation. **f**, Western blot demonstrating the expression level of $GLI3^A$ and $GLI3^R$ protein during cardiomyocyte differentiation. **g**, Relative proportions of GLI^A and GLI^R proteins expressed during cardiomyocyte differentiation.

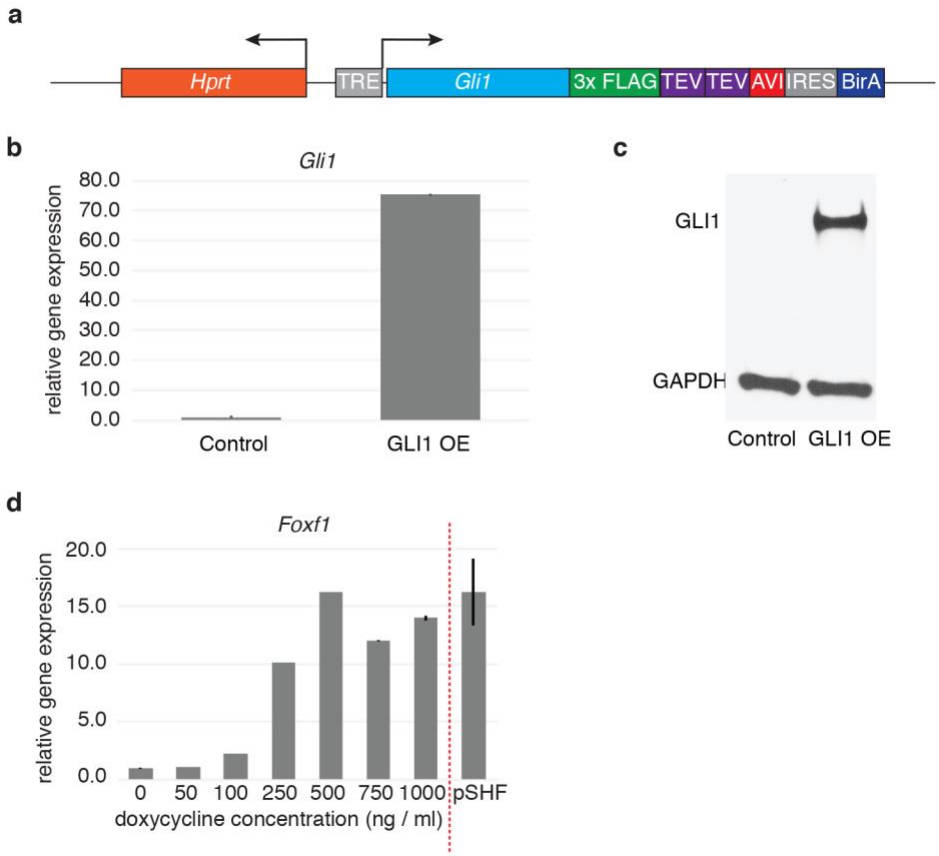

Extended Data Figure 3. GLI1 overexpression in cardiac progenitors leads to activation of pSHF Hedgehog targets. **a**, Schematic representation of the *Gli1-FTA* transgenic cassette inserted into the *Hprt* locus in mESCs. **b**, 500ng/ml doxycycline treatment of the *Gli1-FTA* transgenic line for 24 hours results in robust expression of *Gli1*. **c**, Normally Hh-inactive cardiac progenitors express GLI1 protein after doxycycline treatment for 24 hours, as assessed by western blot. **d**, Relative levels of the Hh target *Foxf1* resulting from different doxycycline concentrations in cardiac progenitors, in relation to endogenous *Foxf1* expression levels in the embryonic pSHF.

a

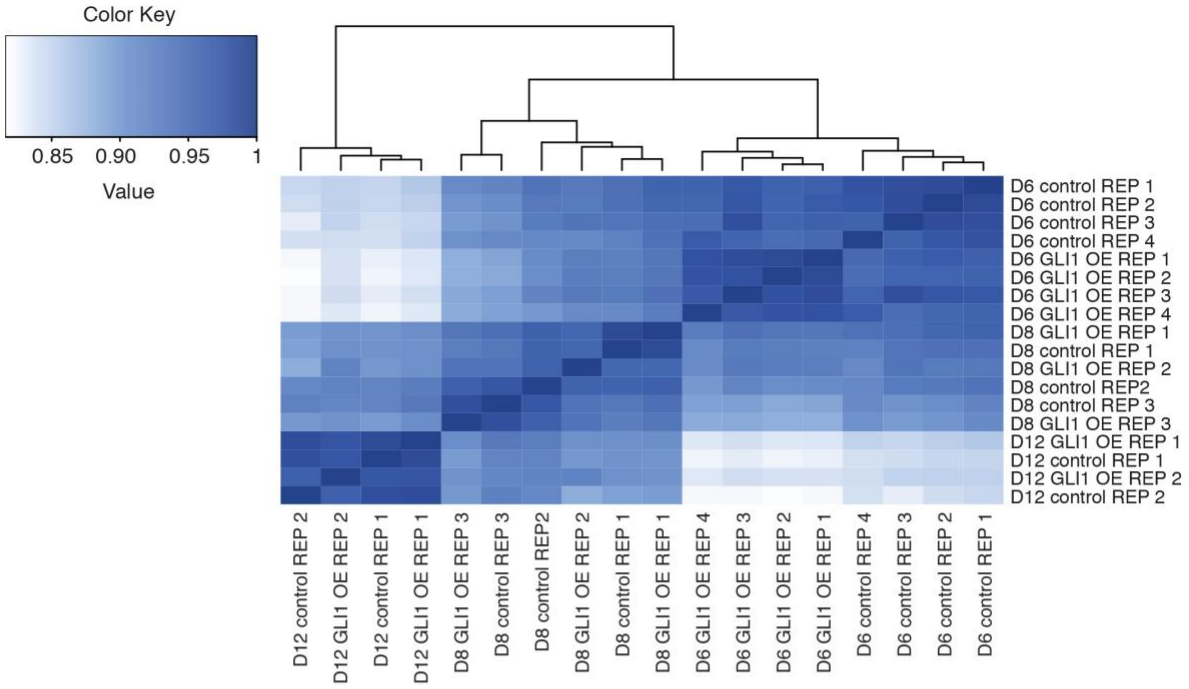

b

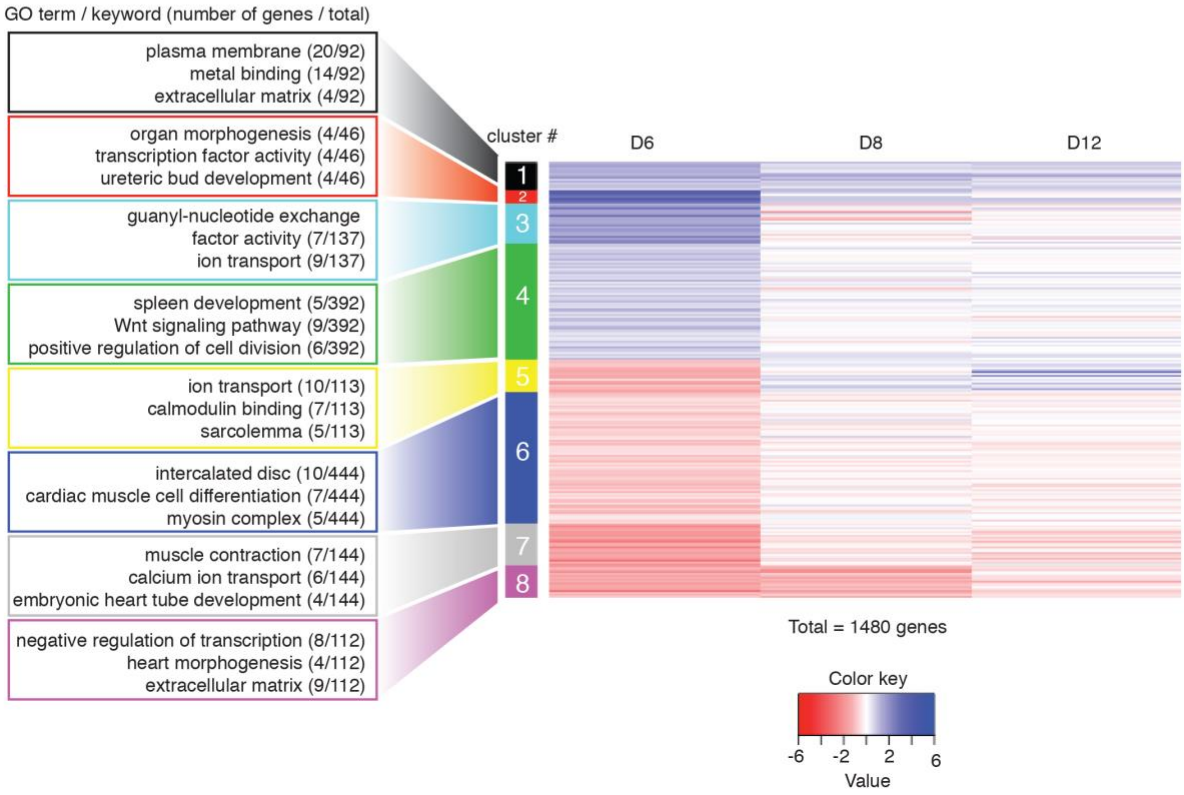

Extended Data Figure 4. Brief GLI1 overexpression in cardiac progenitors results in a transient disruption to the cardiomyocyte differentiation program. **a**, Heatmap displaying correlation of gene expression profiles from GLI1 OE and control cells at all differentiation stages analyzed. Clustering of samples reveals a strong separation of samples by treatment at Day 6, but intercalation of treated with untreated samples at Day 8 and Day 12. **b**, Heatmap time series of genes differentially expressed at Day 6 demonstrates a trend towards normalization of gene expression as differentiation proceeds and cells recover from GLI1 OE. Gene ontology (GO) term analysis reveals that gene clusters containing genes that are transiently upregulated at Day 6 associate with progenitor-related GO terms, while clusters containing genes that are transiently downregulated at Day 6 associate with cardiomyocyte-differentiation related GO terms.

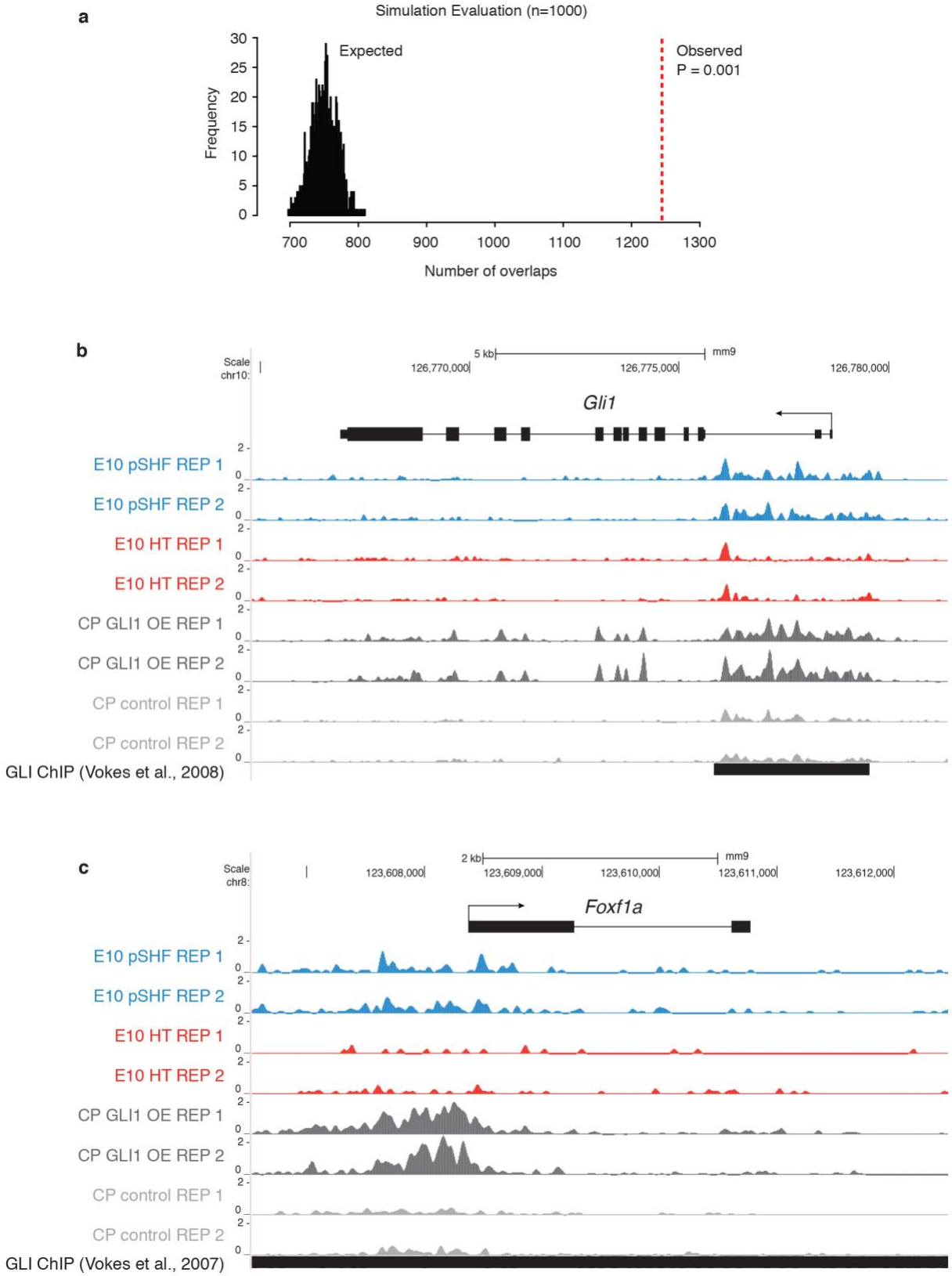

Extended Data Figure 5. Brief GLI1 overexpression in cardiac progenitors results in alterations in the chromatin profile at Hh-dependent genes. **a**, Monte Carlo simulation testing the hypothesis that GLI1 OE-specific accessible chromatin regions are enriched within pSHF-specific embryonic accessible chromatin regions. *P*-value = 0.001. **b**, Replicate ATAC-seq read enrichment and ChIP-seq peaks at the Hh target *Gli1* locus in GLI1 OE and control cardiac progenitor (CP) cells, as well as SHF cardiac progenitors and HT cardiomyocytes. **c**. Replicate ATAC-seq read enrichment and ChIP-seq peaks at the Hh target *Foxf1* locus in GLI1 OE and control cardiac progenitor (CP) cells, as well as SHF cardiac progenitors and HT cardiomyocytes.

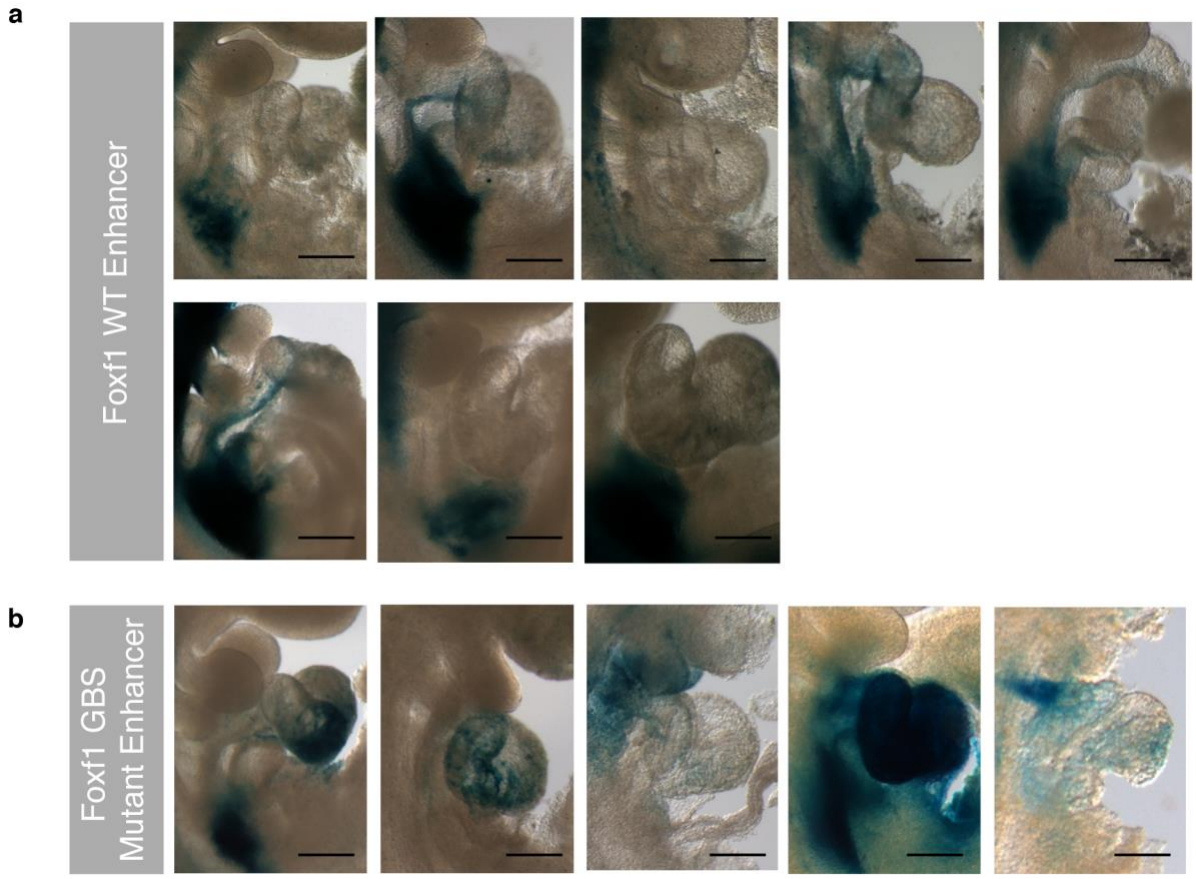

Extended Data Figure 6. GLI binding sites are required for progenitor-specific activity of a distal CRE upstream of Hh-dependent SHF genes. a, transient transgenic analysis of embryos injected with the Hsp68-LacZ vector under the control of the WT *Foxf1* enhancer. **b**, transient transgenic analysis of embryos injected with the Hsp68-LacZ vector under the control of the GBS mutant *Foxf1* enhancer. Scale bar in **a**, **b** = 100um.